Construction of a 3D Metal−Organic Framework and Its Composite for Water Remediation via Selective Adsorption and Photocatalytic Degradation of Hazardous Dye

Arif Ali, Mohd Muslim, Ishita Neogi, Mohd Afzal, Abdullah Alarifi, and Musheer Ahmad*

Read Online

ACCESS | Metrics & More | Article Recommendations | SI Supporting Information

ABSTRACT: In this work, a new bimetallic Na(I)−Zn(II) metal−organic framework (MOF), formulated as $[Na_2Zn_3(btc)_2(\mu\text{-}HCOO)_2(\mu\text{-}H_2O)_8]_n$ (**1**) (H_3btc = benzene tricarboxylic acid), and its composite (ZnO@**1**) have been successfully synthesized using solvothermal and mechanochemical solid grinding methods. **1** and ZnO@**1** were characterized by diffraction [single-crystal X-ray diffraction (XRD) and powder XRD], spectroscopic (ultraviolet−visible diffuse reflectance spectroscopy and Fourier transform infrared spectroscopy), microscopic (transmission electron microscopy), and thermal (thermogravimetric analysis) methods. The surface area and porosity of **1** were determined using a Brunauer−Emmett−Teller analyzer. Single-crystal diffraction of **1** confirms that Na1 and Zn2 have octahedral coordination environments, whereas Zn1 has a tetrahedral coordination geometry. Topological simplification of **1** shows a 3,6-connected ***kgd*** net. Na(I)−Zn(II) MOF (**1**) is crystallized with slight porosity and exhibits good tendency toward the encapsulation of zinc oxide nanoparticles (ZnO NPs). The photocatalytic behaviors of **1** and its composite (ZnO@**1**) were investigated over MB dye under sunlight illumination with promising degradation efficiencies of 93.69% for **1** and 97.53% for ZnO@**1** in 80 min.

1. INTRODUCTION

In the past years, the demand of commercialized dyes and their products has increased rapidly. The bulk production of a variety of dyes was mainly aimed at to fulfill the demand of huge population, but less attention was paid to their discharges and implications on water bodies.[1−3] Near about thousands of natural and organic synthetic dyes and dyestuff are being used in textile, paper, and leather industries for coloring the products and are discharged into water sources. Based on the World Bank reports, ∼17−20% contribution of water pollution is due to the textile and dyeing industries.[4−6] According to recent reports, it has been concluded that the total annual production of azo dyes (−N=N−) accounts for about 7×10^5 tons and ∼13−15% of this value is discarded into the water bodies.[7,8] These waste dyestuff materials are potentially toxic not only to human health but also to environments and aquatic life.[1,9,10] Slow degradation of such dyestuff by sunlight in the water system and further complexation with several essential metal ions may be hazardous for living systems.[11]

Metal−organic frameworks (MOFs) are a new class of crystalline hybrid materials, also famous as brilliant porous coordination materials that are composed of the organic linker and inorganic secondary building units (metal ions/metal nodes).[12−16] MOFs have witnessed fast development in inorganic as well as material chemistry due to their attractive properties, intriguing topologies, and structural features coupled with high surface area, thermal stability, and porosity. Moreover, the conventional semiconductor nature of MOFs is solely dependent on the photoactive organic ligands, which can be tuned by incorporating active metal ions.[17,18] MOFs have been exploited potentially in a wide range of research areas such as photocatalysis,[19−21] adsorption,[8,22−26] gas sorption,[26−30] sensing,[31−33] magnetism,[34−38] and so on. The dimensionality and topology of MOFs are also dependent on their mode of coordination assembly.[39,40] Zhang and co-workers synthesized a new MOF material (NENU-505) that has shown adsorption of cationic dye, and the adsorption capacity of NENU-505 was 33.5 mg/g at room temperature for methylene blue (MB).[41] Li and co-workers have also constructed a new Cu-MOF for the removal of MB dye with a 45.045 mg/g or 96% removal rate.[42a] Abedi and co-workers have also shown the photocatalytic activity of the Ni(II)/K-based heterometallic MOF toward the
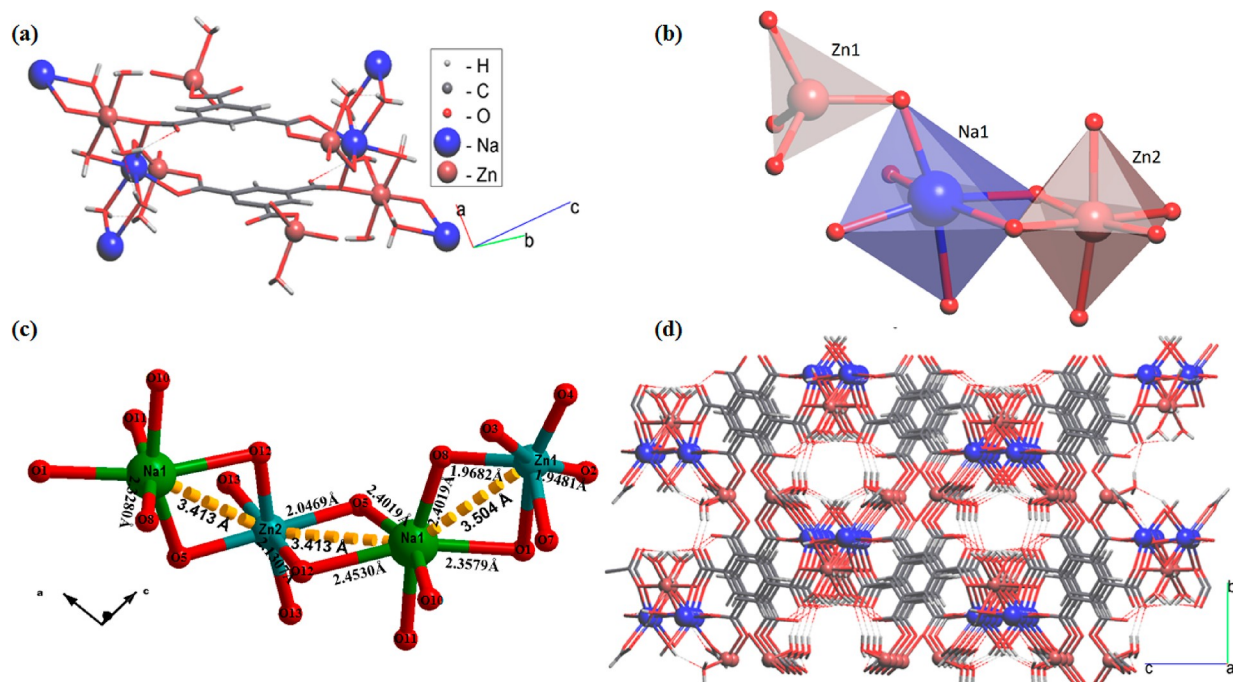
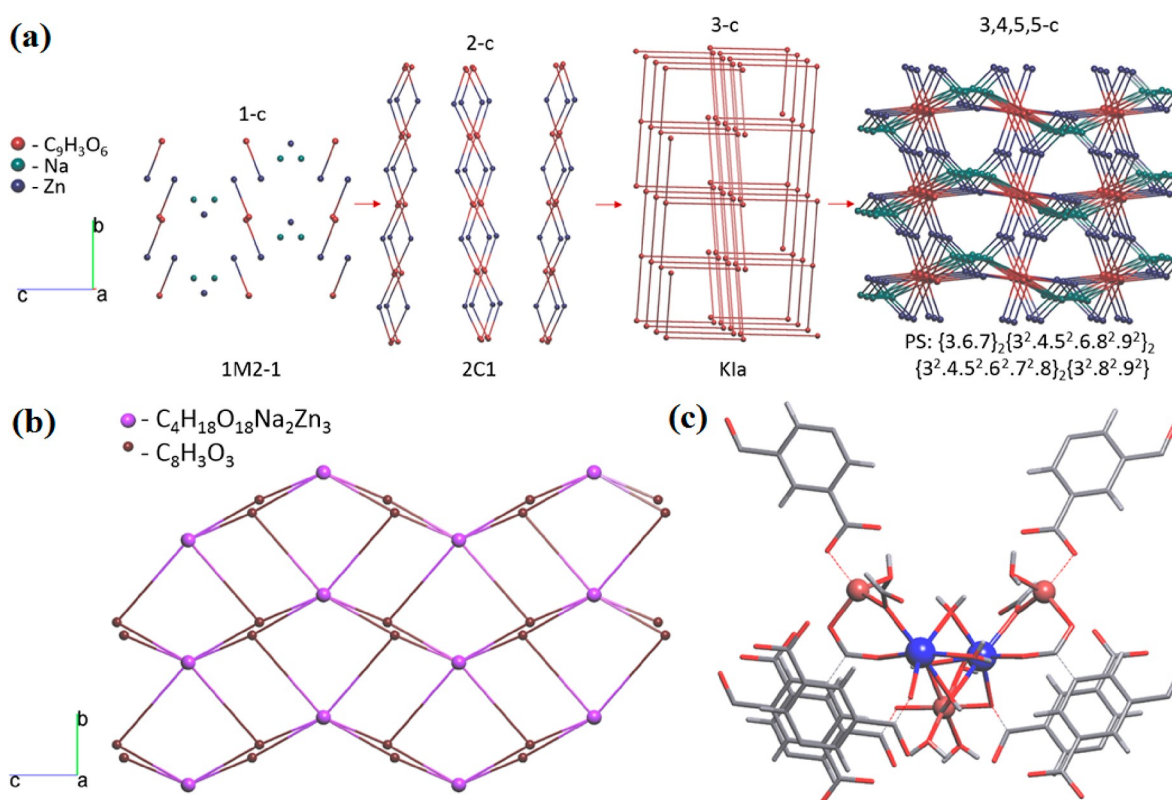**Figure 1.** (a) View of the molecular structure of **1**, (b) polyhedral view of metal ions, (c) linear heterometallic chain of Zn(II) and Na(I) ions, and (d) 3D architecture.


Figure 2. (a) Order of the subnets that describe the packing of the structure on different levels of the solid angle, (b) ***kgd*** topological type after rod−net representation of structure **1**, and (c) structural fragments in the (100) direction.

degradation of bromocresol green (BCG) dye under visible light, which led to 94% degradation.[42b]

MOFs play the most promising role in host−guest chemistry. MOFs that are well-designed and have suitable porosity are capable of hosting the nanoparticles (NPs). NPs are nanosized

materials with a high surface area and good semiconductor properties. Some pioneering researchers have developed a variety of MOF-based NPs (NP@MOFs) via the solid grinding method.[43a−d] They successfully established that the NPs can be encapsulated inside the pores of MOFs via the host−guest
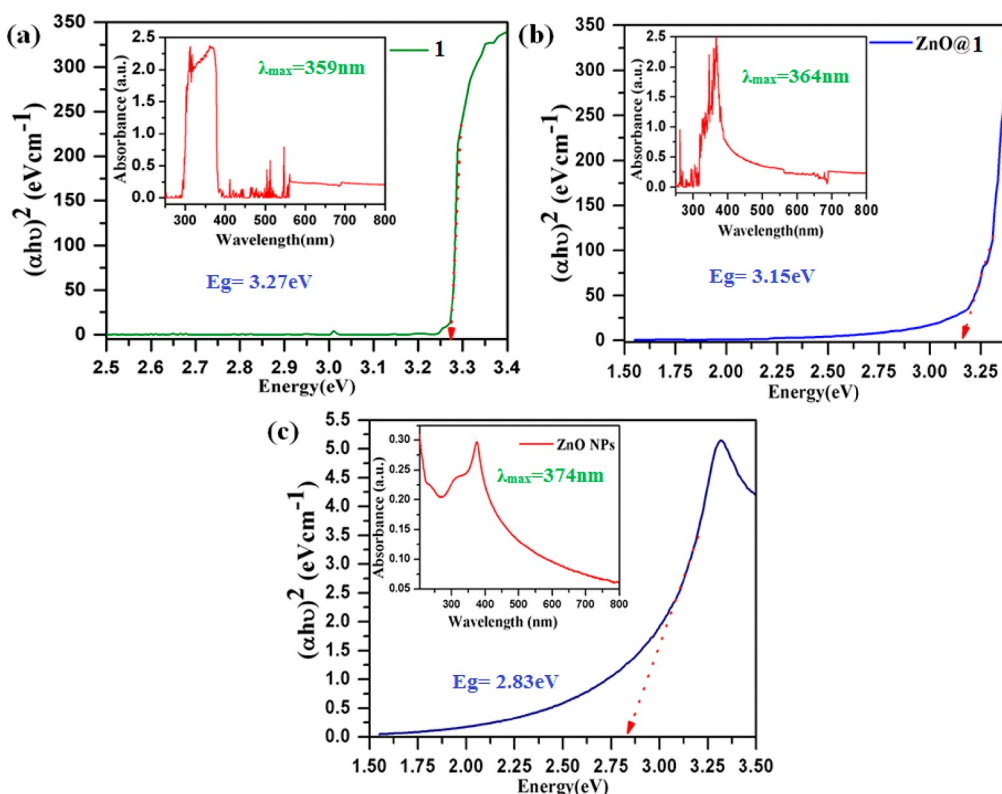
Figure 3. Optical band gaps as estimated from the Tauc plot using UV-DRS spectra (a) **1**, (b) ZnO@**1**, and (c) ZnO NPs.

mechanism, exploiting various non-covalent interactions.[44] Encapsulation of MOFs with NPs could result in decreasing the band gap due to fast (e^-/h^+) recombination between MOF architectures and metal NPs.[45−47] The above observation inspired us to design and synthesize a new ZnO@**1** composite via the solid grinding method, and it shows promising MB dye degradation efficiency over the MOF (**1**).

2. RESULTS AND DISCUSSION

**2.1. Structural Description and Topological Study of MOF 1.** The crystal structure of $[Na_2Zn_3(btc)_2(\mu\text{-}HCOO)_2(\mu\text{-}H_2O)_8]_n$ (**1**) was confirmed by single-crystal X-ray diffraction (XRD), and it was crystallized in the monoclinic system with the $C2/c$ space group. The asymmetric unit of **1** consists of one benzenetricarboxylate ion (organic linker), four water molecules (three coordinated and one μ-H$_2$O), two independent zinc metal ions, and one sodium ion (Figure 1a). The fully deprotonated (btc^{3-}) ligand adopts both the mono and bidentate fashion to connect Zn(II) and Na(I) ions. However, the formate (HCOO$^-$) adopts the bridging monodentate fashion with Zn(II) and Na(I) ions. Na1 and Zn2 have octahedral coordination polyhedra (CN = 6), and Zn1 has a tetrahedral coordination polyhedron (Figure 1b). As depicted in Figure 1c, MOF **1** shows the following bond lengths: Zn1−O2 = 1.9481 Å, Zn1−O8 = 1.9682 Å, Zn2−O5 = 2.0469 Å, Zn2−O12 = 2.1307 Å, Na1−O1 = 2.3579 Å, Na1−O5 = 2.4019 Å, Na1−O8 = 2.3280 Å, Na1−O12 = 2.4530 and Zn1−Na1 = 3.504 Å, and Zn2−Na1 = 3.413 Å, which are within the reported range. The linear chain of Zn(II) and Na(I) is further extended by carboxylates of btc^{3-} ligands to generate a three-dimensional heterobimetallic architecture (Figure 1d).

The topological study of **1** shows the coordination formula to be $A_5K^5{}_2M^2{}_6M^1{}_4$,[48] where A is a metal $[(Zn)_3$ and $(Na)_2]$, K^5 is

$C_9H_3O_6$, M^2 is CHO$_2$, and M^1 corresponds to water. The standard representation of valence-bonded **1** in the 3,4,5,5-c nodal net of the new topological type with the point symbol for the net is represented as follows: $\{3.6.7\}_2\{3^2.4.5^2.6.8^2.9^2\}_2\{3^2.4.5^2.6^2.7^2.8\}_2\{3^2.8^2.9^2\}$ (Figure S1). To understand the extended generation of different subnets from the underlying net that contains the edges of weight no less than a specified value and having applied the multilevel analysis following the order of subnets, we describe the packing of the structure on different levels of solid angle (Supporting Information, Table S1). At a higher solid angle, the coordination of **1** is zero-dimensional (0D). On decreasing the solid angle, we have found extended dimension packing of the structure connected. Formation of a 3,4,5,5-c net depends on the value of the solid angle (Ω_i), as shown in Figure 2a. The **kgd** topology in a 3,6-connected net with the point symbol for net $\{4^3\}_2\{4^6.6^6.8^3\}$ is presented in Figure 2b,c.

2.2. FTIR, PXRD, TGA, and UV-DRS Analysis. The vibrational bands show the binding of carboxylate, formate (μ-HCOO$^-$), and water (μ-H$_2$O) with sodium and zinc metal ions. Herein, the vibration stretching frequency of ν(O−H) of the bridging water molecules is observed at 3360 cm^{-1}. The medium absorption bands ∼2800−3127 cm^{-1} could be due to the hydrogen-bonded −OH network inside the MOF. The absorption frequencies at ∼2750 and 1340 cm^{-1} may be attributed to the stretching and bending vibrations of bridging formate (HCOO$^-$) ions.[8,49] The symmetric and asymmetric vibrational bands at 1412 cm^{-1} [ν_s(COO$^-$)] and 1595 cm^{-1}[ν_{as}(COO$^-$)] could be assigned to the carboxylate groups.[50−52] The absorption bands ν(Na−O) and ν(Zn−O) appeared at 561 and 466 cm^{-1}, respectively. Similarly, ZnO@**1** shows shifting in the characteristic absorption bands. The absorption band at 3450 cm^{-1} could be attributed to ν(O−H),
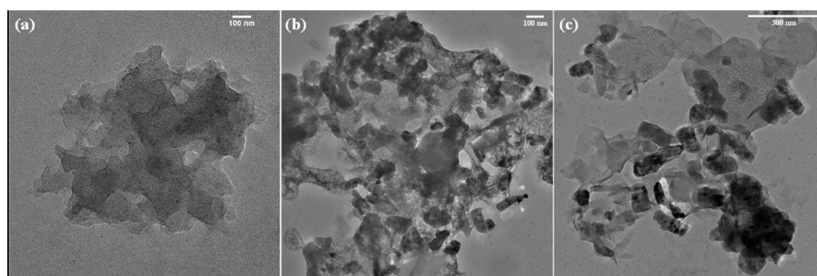
Figure 4. TEM images of (a)MOF **1**, (b) ZnO@**1** at low magnification, and (c) ZnO@**1** at high magnification.
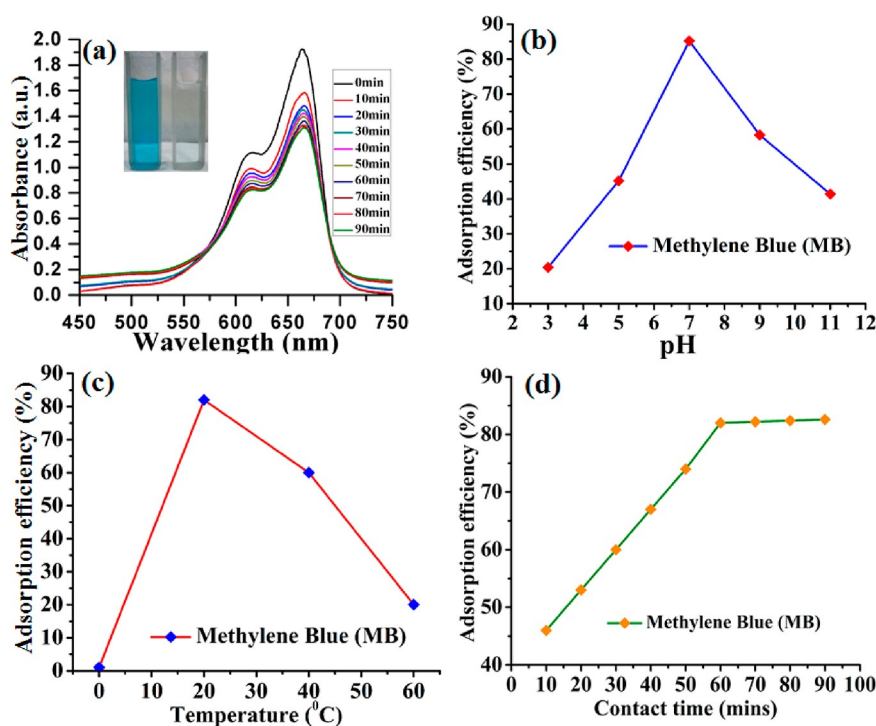
Figure 5. (a) UV−vis absorption spectra of **1** for MB dye uptake, (b) removal efficiency at variable pH values, (c) effect of temperature, and (d) effect of contact time.

and the disappearance of the band at 3127 cm^{-1} indicates that zinc oxide NPs (ZnO-NPs) are encapsulated inside the pores via hydrogen bonding and other weak interactions.[53] The vibrational absorption band at 475 cm^{-1} could be due to ZnO NPs[54] (Figure S2).

Powder XRD (PXRD) patterns were recorded to check the bulk phase purity or structural integrity of **1** and ZnO@**1**. Simulated and experimental patterns match well, which confirm the bulk purity of the synthesized MOF. ZnO@**1** shows new patterns from 25 to 40°, which could be an indication of the embedding of zinc oxide NPs inside the pores of **1**. The structural integrity and crystalline nature of the architecture were maintained during the experiments (Figure S3). Thermogravimetric analysis (TGA) was performed to confirm the thermal stabilities of **1** and its composite (ZnO@**1**). The decomposition of the framework of **1** started at ~115 °C due to the elimination of coordinated water molecules. MOFs **1** and ZnO@**1** are thermally stable upto ~290 °C and ~315 °C, respectively (Figure S4).

Ultraviolet−visible diffuse reflectance spectroscopy (UV-DRS) spectra of **1** and its composite were recorded between 250 and 800 nm to identify their optical behaviors. The energy band gap of **1** and its composite were estimated from the Tauc

plot. The plot of $(\alpha h\nu)^2$ versus the energy $(h\nu)$ gives the band gap as the x-axis intercept of an extrapolated tangential line.[9] The band gaps of **1** and its composite were estimated to be 3.27 and 3.15 eV (Figure 3a,b), respectively. Moreover, zinc oxide NPs show a band gap energy of 2.83 eV (Figure 3c).

2.3. BET and TEM Analyses. The specific surface area and porosity of **1** were determined using Brunauer−Emmett−Teller (BET) adsorption isotherms for N_2 gas at 77 K and pore size distribution evaluated from the non-local density functional theory (NLDFT) equilibrium model.[55] Degassed MOF **1** exhibited slight porosity with variable pore volume distributions (Figure S5).

MOF **1** and ZnO@**1** have different particle sizes and morphologies that were confirmed by the transmission electron microscopy (TEM) analysis (JEOL JEM-2100F). Figure 4a depicts particles of **1** to be in a fractured cage-like architecture, which get encapsulated with ZnO NPs.[43b,c,56] To give better insights into ZnO@**1**, both low-magnification (Figure 4b) and high-magnification (Figure 4c) images were recorded.

2.4. Dye Adsorption Studies. For this purpose, crystals of **1** were soaked in the aqueous solution of MB and methyl orange (MO) dyes of 15 ppm concentration at room temperature for 12 h.[57a] The changes in concentrations of the MB and MO dyes in

Table 1. Kinetic Parameters of MB Dye Adsorption for 1

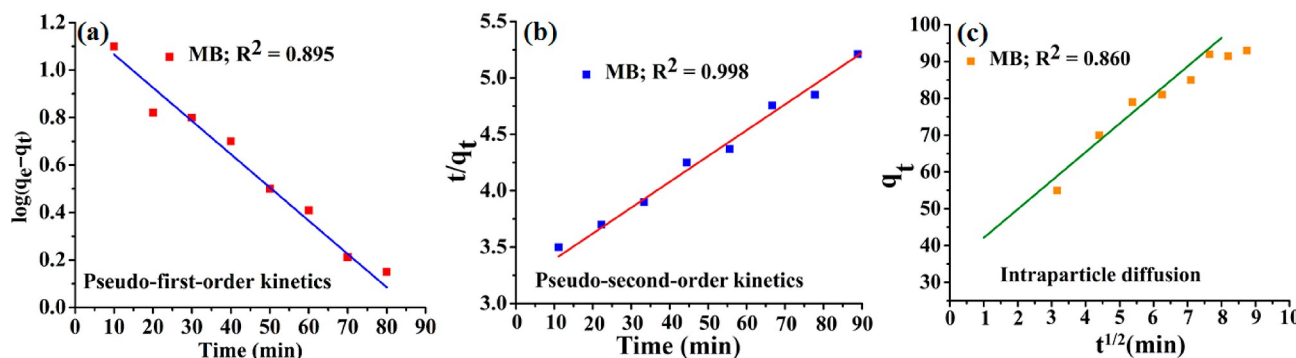| model	pseudo-first-order kinetics				pseudo-second-order kinetics				intraparticle diffusion	
parameter	k_1 (min^{-1})	q_e (cal) (mg/g)	q_e (exp) (mg/g)	R^2	k_2 (g mg^{-1}min^{-1})	q_e (cal) (mg/g)	q_e (exp) (mg/g)	R^2	k_3 (mg/g min$^{-1/2}$)	R^2
MB	0.36	140.30	120.28	0.895	0.065	280.50	290.7	0.998	34.6	0.860

Figure 6. Adsorption kinetic plots for MB dye adsorption on **1**: (a) pseudo-first-order, (b) pseudo-second-order, and (c) intraparticle diffusion models.

the solution were measured using a UV−visible (UV−vis) spectrophotometer. The color visual and UV−vis absorption spectra of MB and MO dye solution revealed that MO dye showed a negligible change in absorption intensity with its maximum absorption wavelength (464 nm) (Figure S6). Interestingly, the selective adsorptive binding of cationic MB dye molecules on the framework of **1** could be directed by the formate ions and carboxylate oxygen atoms of btc^{3-} ligands through electrostatic, π−π, and hydrogen bonding interactions (Figure S7 and Supporting Information, Table S2).[8,57b,58] Therefore, the adsorption experiment proceeded on the selected MB dye only.

To understand the adsorption phenomenon of **1**, batch adsorption experiments were performed, which give the important insights into the adsorption efficiency, kinetics, and adsorption mechanism.[59,60a] Figure 5a depicts the UV−vis spectra of **1** before and after adsorption of the MB dye. MB was adsorbed to the maximum extent of **1** with an adsorption efficiency of 78% within 10 mins of the adsorption experiment. However, an equilibrium condition could be attained after achieving 85.2% adsorption efficiency; afterward, MOF **1** showed saturation due to the limitation of adsorption sites on it.[60b]

To investigate how the MB dye is being adsorbed, we took photographs of cuvettes containing the dye solution after isolating MOF **1** from it. Additionally, the scavenging effect of the MB dye adsorption on **1** was confirmed by UV−vis characteristic peaks at 664 nm with a decreasing trend of absorption intensity at the same wavelength.[60c] To confirm the structural integrity of **1**, we recorded PXRD data before and after adsorption of MB dye on it (Figure S3). There is no significant variation observed in diffraction patterns with a slight change in the peak intensity. Therefore, it is confirmed that **1** facilitates dye adsorption without losing its crystallinity after adsorption.[61a,b]

2.5. Adsorption Kinetics. To analyze the adsorption kinetics, the experimental data were fitted with adsorption kinetic models, such as pseudo-first-order, pseudo-second-order, and intraparticle diffusion kinetic models.[61c] Several batches of experiments were carried out to investigate the rates of adsorption, which depend upon the mobility of the dye

molecules onto the surface of **1**.[61d] By using the models, the values of kinetic parameters and the correlation coefficient can be calculated with the help of the following equations, eqs 1−3, respectively.[61d]

$$\log(q_e - q_t) = q_e - \frac{k_1}{2.303} \tag{1}$$

$$\frac{1}{q} = \frac{1}{k_2 q_e^2} + \frac{t}{q_t} \tag{2}$$

$$q_t = k_3 t^{1/2} \tag{3}$$

Here, the adsorption capacity of **1** is described by q_e and q_t (mg/g) at the equilibrium and time. Rate constants are different for different orders of the reaction such as k_1 for the pseudo-first-order model (min^{-1}), k_2 for the pseudo-second-order model (g mg^{-1} min^{-1}), and k_3 for the intraparticle diffusion model (mg g^{-1} min^{-1}).[62,63]

The fitting results such as the adsorption capacities, rate constant, and correlation coefficient are shown in Table 1. The correlation coefficient (R^2) values of **1** at different initial concentrations were all <0.998 through the pseudo-second-order model.[64a,b] The good linear fitting relationship supported that the pseudo-second-order kinetic model was the fitting model for calculating the amount of MB in a short period (Figure 6). The highest adsorption amount of MB could reach up to 290.7 mg/g, which was comparable to those of the reported MOF architecture (Table 3).[64c]

2.6. Effect of pH. pH is an important parameter influencing the adsorption process by changing the surface charge distribution of the adsorbent.[65−68,69a] To gain deep insights into the influence of pH on the adsorption process, we prepared a series of solution of **1** with pH values in the range ∼3.0−14.0. The pH values were adjusted using 0.1 N NaOH and 0.1 N HCl solution in an aqueous medium under ambient conditions.[69b] It is evident from Figure 5b that as we increase the pH from 3 to 7, the adsorption capacity of **1** increases significantly. At a low pH of 3, **1** achieved ∼20% adsorption efficiency due to the interaction of the H$^+$ ions with the positive part of MB dye.[62] However, 85.2% adsorption efficiency is reached at pH = 7.

Conversely, as we increase the pH range from neutral to alkaline, pH = 11, it can be seen that the adsorption capacity (~42%) decreases significantly due to the negative part of MB interacting with the base forming NaCl.[63,69c,70,71a] The effect of pH on the uptake capacity has been shown with **1** being a better adsorbent at a pH of 7 with 85.2% removal efficiency of MB dye.

To identify the surface charge of the **1** adsorbent, the point of zero charge (PZC) (pH_pzc) method was utilized.[71b] The PZC (pH_pzc) value can be estimated from the plot between initial pH and ΔpH (initial pH − final pH), which is ~6.7 in the case of MOF **1** (Figure 7). It is observed[71c,d] that the negative charge on

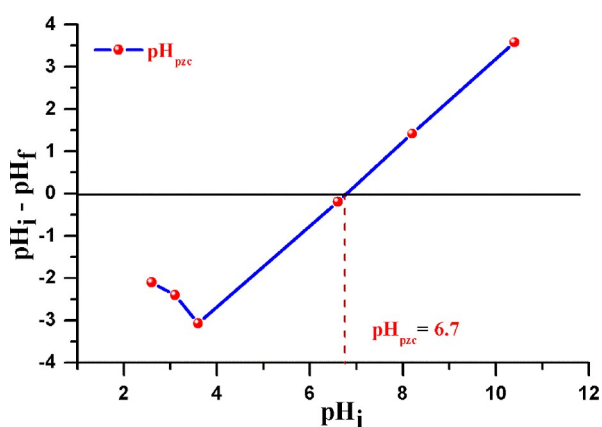**Figure 7.** PZC (pH_PZC) plot for **1**.

the surface of the adsorbent gets accumulated with the increase in the pH, resulting in the adsorption of cationic dyes on its surface being favored.

2.7. Effect of Temperature.
The temperature of the solution phase is considered to be a significant parameter because it changes the adsorption capacity of the adsorbent.[72a,b,73] The effect of temperature on the adsorption efficiency of **1** was recorded at different temperatures ranging from 20 to 60 °C (Figure 5c). The maximum adsorption efficiency (82%) of **1** was observed at room temperature (20 °C), and it started to decline with further increase in the temperature from 20 to 55 °C, which indicates an exothermic process.[74a,b,75]

2.8. Effect of Contact Time.
The contact time is also an important factor that influences the adsorption capacity of the adsorbents.[76a] At the start of the reaction time, $t = 0$ min, **1** shows a negligible amount of MB dye adsorption. However, ~45% MB dye adsorption was achieved during the first 10 min of contact time. A rapid adsorption process was recorded during the first 60 min of adsorption. After this period, the equilibrium is reached with 82.5% adsorption efficiency, and beyond it, saturation is observed (Figure 5d).[76b,c,77,78]

2.9. Photocatalytic Activity.
Furthermore, for the complete remediation of unabsorbed MB dye from wastewater, the photocatalytic process has been proved to be an efficient method to degrade or mineralize the organic pollutants from wastewater under sunlight.[79,80] Therefore, we performed photocatalytic degradation of MB dye over **1** and ZnO@**1** by using batch experiments that have shown a characteristic change in UV−vis absorbance upon sunlight illumination. UV−vis experiments have shown a gradual change in the intensity of the dye solution under photoirradiation, which indicates the successful photocatalytic degradation of dye molecules (Figure 8a,d). Photocatalytic degradation of MB was estimated from the absorption intensity versus irradiation time plot at $\lambda_{max} = $ ~664 nm (Figure 8b,e). Dye degradation efficiencies over **1** and ZnO@**1** were calculated using the following relation (eq 4).[81]
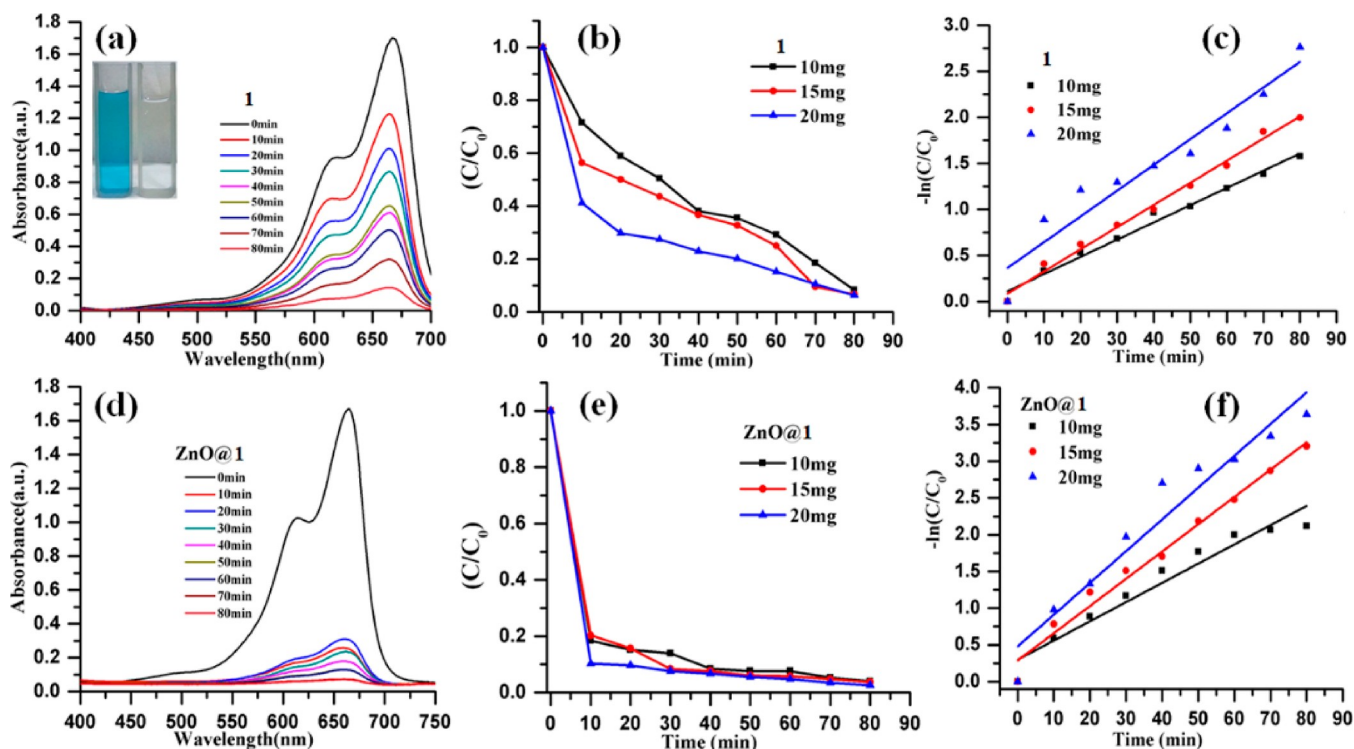

Figure 8. (a,d) UV−vis spectra of the change in MB dye concentrations over **1** and ZnO@**1**, (b,e) photocatalytic degradation of MB dye with time in an aqueous solution under sunlight irradiation, and (c,f) kinetics of MB dye degradation, plot of $-\ln(C_0/C)$ vs time (min).

Photocatalytic degradation efficiency (%)

$$\frac{(C_0 - C)}{C_0} \times 100 \qquad (4)$$

where the initial concentration is represented by C_0 and the final concentration is represented by C at time t.

Overall degradation values of MB dye over **1** and ZnO@**1** were observed to be 93.69 and 97.53%, respectively.

For **1**, degradation values of MB over 10, 15, and 20 mg were obtained to be 27.83, 46.66, and 58.81% for the initial 10 min, respectively, and the overall percentage were 91.53, 93.26, and 93.69% within 80 min, respectively. Similarly, ZnO@**1** has shown degradation of 81.60, 79.68, and 89.75% within the first 10 min and 95.92, 97.30, and 97.53% within 80 min, respectively.

Moreover, the degradation kinetics of MB dye was evaluated by using the Langmuir–Hinshelwood mechanism. Photocatalytic degradation of MB dye followed pseudo-first-order kinetics

$$\ln C = -kt + \ln C_0 \qquad (5)$$

where the initial dye concentration is C_0 (mg/L) at time $t = 0$, the final dye concentration is C (mg/L) at time $t = t$ (min), and k is the dye degradation rate for the catalyst of pseudo-first order, and on simplifying eq 5,

$$\ln(C_0/C) = kt \qquad (6)$$

where, the rate of degradation $-\ln(C/C_0)$ versus irradiation time shows linear fitting for MB dye as per eq 6. The apparent rate of the reaction was obtained using eq 7, which shows the degradation rate of the reaction for dye[82,83]

$$\frac{1}{k_{app}} = \frac{1}{k_r k_{L-H}} + \frac{C_0}{k_r} \qquad (7)$$

where C_0 is the initial dye concentration, k_{app} is the apparent adsorption constant for MB dye on the surface of the photocatalyst (L/mg), the maximum photocatalytic degradation rate (mg/L min) is represented by k_r, and $t_{1/2}$ is the half-life time of the reaction rate, which is calculated by using the following equation, eq 8 (Table 2)[82]

$$\text{half} - \text{life time } (t_{1/2}) = \ln 2/k_{app} \qquad (8)$$

Linear fitting of the plot between $-\ln(C/C_0)$ versus time gives a straight line with a slope parameter value which is equal to the apparent rate constant of pseudo-first-order reaction (k_{app}) (Figure 8c,f). The calculated values of k_{app} for **1** and ZnO@**1** show that the reaction rate increase with the increasing catalyst

dose for MB dye. The half-life time ($t_{1/2}$) of reactions decreased with the increasing catalyst dose, which may be attributed to faster degradation of dye molecules at a 20 mg dose of **1** and ZnO@**1**. Moreover, to understand the better correlation between the catalyst dose and reaction rate, the correlation coefficient (R^2) was considered. The R^2 value of the 15 mg catalyst dose (0.9903 for **1** and 0.9787 for ZnO@**1**) proved its higher efficiency for degradation of MB dye. Therefore, the amount of the catalyst and concentration of dye play a pivotal role in the good heterogeneous recombination for photocatalytic degradation of dye molecules. It is observed that the formation of the electron–hole (e^-/h^+) heterojunction is closely related to the degree of availability of catalyst active sites, which results in successful photocatalysis under sunlight exposure. The tabulated MOFs have displayed good photocatalytic activity for degradation of MB dye under light sources (Table 3).

2.10. Photocatalytic Mechanism for Dye Degradation. MOFs as a semiconducting catalyst can absorb photons and generate electron–hole pairs in conduction and valance bands.[83–85] Upon irradiation of sunlight, the organic linkers act as an electron-releasing agent *via* a conjugation system to metal ions.[86] The hopping of electrons from one place to another place triggers the redox mechanism. Herein, we assume that under the illumination of sunlight, the excited electrons from the ligand system could react with molecular oxygen, forming reactive oxygen species (ROS). Similarly, water molecules and their hydroxyl ions react with the holes and form reactive hydroxyl radicals (OH•).[85–87] Therefore, ROS and OH⁻ radicals play a central role in the degradation of MB dye molecules (Figure 9). According to some recent reports,[88–90] presumably, the lower band gap energy of ZnO@**1** could facilitate the electron excitation at a lower energy and hence fast production of ROS and OH• radicals, which results in an enhanced rate of photodegradation of MB dye molecules.[91,92]

3. CONCLUSIONS

Here, we have summarized the synthesis of Na(I) and Zn(II)-based bimetallic MOF and its composite (ZnO@**1**) under solvothermal and mechanochemical solid grinding methods. Both the MOF **1** and its composite are thoroughly characterized by various spectroscopic, thermal, and microscopic techniques. MOF **1** proved to be a potential adsorbent toward selective removal of cationic MB dyes. The formate ions and carboxylate oxygen atoms of btc³⁻ ligands are key components for the selective adsorptive binding of cationic MB dye molecules on the framework of **1** through several electrostatic and non-covalent interactions. **1** and its composite have exhibited promising photocatalytic degradation activity of MB dye under sunlight illumination.

4. EXPERIMENTAL SECTION

4.1. Materials. Benzenetricarboxylic acid (H₃btc), zinc nitrate [Zn(NO₃)·6H₂O], sodium formate (HCOONa), and potassium nitrate were procured from Sigma-Aldrich. Sodium hydroxide, MB dye, and solvents were purchased from Fisher Scientific and used as received.

4.2. Instrumentation. A CE-440 elemental analyzer (Exeter Analytical Inc.) was used for elemental analysis of MOF **1**. Photocatalytic degradation and adsorption studies were performed on a Thermo Scientific Evolution 201 UV–vis spectrophotometer with a standard path length (1 cm) of

Table 2. Apparent Rate Constant (k_{app}), Half-Life Time of the Reaction Rate ($t_{1/2}$), and the Corresponding Correlation Factor (R^2) for Degradation of MB Dye over the Catalyst (1 and ZnO@1), with Values Obtained from the Langmuir–Hinshelwood Rate Equation

	parameters					
	1			ZnO@**1**		
catalyst dose	k_{app} (min⁻¹)	$t_{1/2}$ (min⁻¹)	R^2	k_{app} (min⁻¹)	$t_{1/2}$ (min⁻¹)	R^2
10 mg	0.0187	37.48	0.9843	0.0262	26.46	0.9347
15 mg	0.0241	28.79	0.9903	0.0371	18.67	0.9788
20 mg	0.0280	24.75	0.9178	0.0433	16.02	0.9329

Table 3. Adsorption and Photocatalytic Degradation of MB Dye over 1

MOFs	adsorption				catalyst (MOF)	photocatalytic degradation			
	q_e (mg/g)	kinetics order	mechanism	references		degradation efficiency (%)	source	time (min)	references
UiO-66	69.8	pseudo-second-order	π–π stacking interaction	59	3D Cu based	50	sunlight	210	60
MIL-53(Al)–NH$_2$	45.2	pseudo-second-order	π–π stacking interaction, H-bonding	77	3D Zn based	89	UV light	80	84
MIL-53(Al)	3.6	pseudo-second-order	π–π stacking interaction, H-bonding	77	3D Zn based	63	visible	50	93
SCNU-Z2	455.6	pseudo-second-order	cation-exchange process	90	3D Zn based	79	visible	90	94
3D Na(I)–Zn(II) MOF (1)	290.7	pseudo-second-order	π–π stacking interaction, H-bonding	this work	3D Na(I)–Zn(II) MOF (1)/ZnO@1	93.69/97.53	sunlight	80	this work

cuvettes at ambient temperature. Fourier transform infrared (FTIR) spectra of **1** and ZnO@**1** were obtained using a Thermo Scientific NICOLET model (iS50). UV-DRS spectra were recorded on a PerkinElmer, Lambda 35 spectrophotometer instrument to estimate the optical assets of (**1** and ZnO@**1**) photocatalysts. TGA curves of **1** and its composite were recorded on a Shimadzu TGA-50H instrument. For phase purity of **1** and ZnO@**1**, a Miniflexll X-ray diffractometer was used to record the PXRD pattern. To investigate the particle heterostructure and intimate contact morphology of **1** and its composite, a transmission electron microscopy (TEM) JEOL JEM-2100F instrument was utilized. A Quanta chrome Quadrasorb SI analyzer was used for BET analysis.

4.3. Single-Crystal Diffraction Details. The diffraction data of **1** were obtained on a Bruker SMART APEX CCD diffractometer and collected using monochromatic Mo Kα radiation ($\lambda = 0.71073$ Å) at 100(2) K. The linear absorption coefficients and the anomalous dispersion corrections were obtained from the International Tables for X-ray crystallography.[95] Using Olex2,[96] the structure was solved using the olex2. Solve[97] structure solution program using Charge Flipping and refined using the olex2. Refine[97] refinement package using Gauss−Newton minimization. All hydrogen atoms were located in different Fourier maps in the structures and refined isotropically. All non-H atoms were refined anisotropically. The crystal structural refinement data, details of the bond lengths, and bond angles of **1** are provided in Supporting Information, Tables S3−S5.

4.4. Synthesis of Complex 1. A mixture of 20 mg of benzenetricarboxylic acid (H$_3$btc), 10 mg of sodium formate (HCOONa), and 100 mg of zinc nitrate [Zn(NO$_3$)$_2$·6H$_2$O] was dissolved in 5 mL of the solvent mixture (2 mL of ethanol and 3 mL of H$_2$O) and transferred into a Teflon autoclave. 0.5 mL of sodium hydroxide solution (1 mmol) was added into it and sealed tightly. The autoclave was placed in the hydrothermal oven for 72 h at 120 °C. After this period, we obtained a pale yellow colored solution, and it was filtered. The solution was left to allow slow evaporation. After 2−3 weeks, we observed light pale yellow cubic-like crystals (Scheme 1). Melting point: 245 °C; elemental analysis (%): calcd for C$_{20}$H$_{24}$Na$_2$O$_{24}$Zn$_3$ (890.57): C, 26.97%; H, 2.72%; found: C, 27.01%; H, 2.79%. IR (cm^{-1}): 3359 (w), 3127 (w), 2800 (m), 2460 (w), 1586 (s), 1456 (s), 1379 (s), 1113 (w), 1017 (s), 880 (w), 820 (w), 768 (m), 716 (m), 561 (m), 466 (w).

4.4.1. Synthesis of ZnO@1. Zinc oxide NPs (ZnO NPs) and ZnO@**1** were synthesized using earlier reported procedures with slight modification.[43,47,98] We took 100 mg of MOF **1** and 10% (w/w) of zinc oxide NPs in an agate mortar and pestle and performed mechanochemical solid grinding for 2 h at ambient temperature. Following this, a few drops of ethanol in ground powder were added and subjected to drying under vacuum for 30 min. The obtained ZnO@**1**, as shown in Scheme 2, is thoroughly characterized. IR (cm^{-1}): 3450 (s), 2850 (w), 2460(w), 1620 (s), 1477(s), 1376 (m), 1343 (m), 1190 (w), 1119 (s), 1017 (s), 840 (w), 768 (w), 725 (w), 622 (w).

4.5. Batch Adsorption Process. We prepared a standard stock solution of 15 ppm [15 mg of the dye in 1 L of demineralized water (DMW)] MB dye. The crystalline sample of **1** was immersed in 30 mL of dye solution in a 100 mL conical flask and kept for 90 min at room temperature. Following this, we recorded UV−vis spectra between 450 and 750 nm wavelengths at a regular time interval (after each 10 min). The maximum absorption of the dye solution appears at a wavelength
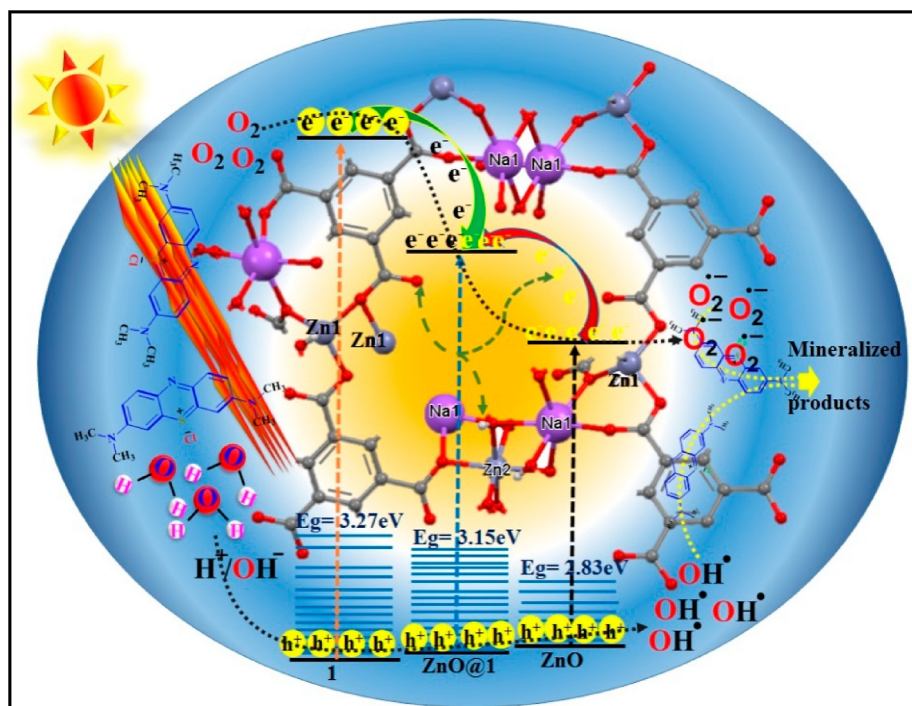
Figure 9. Plausible mechanism of photocatalytic degradation of MB dye over **1** and ZnO@**1** catalysts. Hydrogen atoms are omitted for structural clarity of **1**.

Scheme 1. Schematic Representation of Synthesis of 1
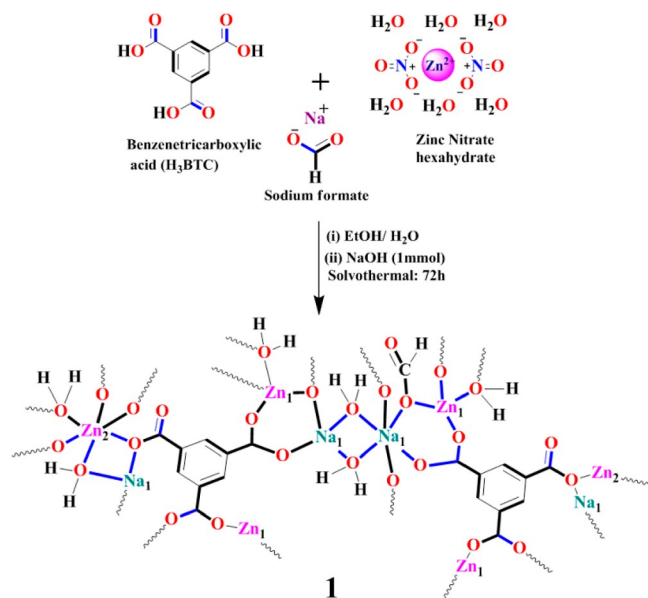
of $\lambda_{\max} = 665$ nm. Moreover, decreasing patterns were observed in the absorbance peak with time. Using eqs 9 and 10,[82] the percentage removal efficiency and the adsorption capacity, respectively, of **1** can be estimated

$$\text{efficiency (\%)} = \left(\frac{C_0 - C_e}{C_0}\right) \times 100 \tag{9}$$

$$q_e = \left(\frac{C_0 - C_t}{m}\right) \cdot V \tag{10}$$

where C_0 (mg/L) and C_t (mg/L) represent the initial and at time t (min) equilibrium concentrations of the dye solution,

respectively. Here, the sample volume is V (in mL) and "m" stands for the dose or mass (mg) of the adsorbent. We also explored the significance of parameters such as time, temperature, and pH on the adsorption process.

4.6. Photocatalytic Degradation of Dye. To check the photocatalytic activity, we took 10, 15, and 20 mg amounts of **1** and ZnO@**1** dispersed in 30 mL of MB dye stock aqueous solution (15 ppm) in 50 mL separate beakers, and before using sunlight irradiation, the solution was magnetically stirred for 1 h to confirm the establishment of the equilibrium between adsorption and desorption processes after the suspended solution was formed. Following this, the solution was exposed to sunlight for photocatalytic degradation of MB dye molecules over **1** and ZnO@**1**, and their UV−vis spectra were continually recorded to confirm absorption behaviors. A continuous decrease in the intensity of the absorption edge confirmed the photocatalytic degradation of MB dye. The overall reaction was shown to follow pseudo-first-order kinetics for photocatalytic dye degradation and the rate constant of the reaction was calculated using eq 11.[98]

$$\ln(C_0/C) = kt \tag{11}$$

where k is calculated from the plot of $-\ln(C/C_0)$ versus time interval and C_0 and C denote the concentrations of dye at time $t = 0$ and $t = t$ (min), respectively.

4.7. PZC Study. To determine the surface charge of adsorbent **1** for the dye adsorption process, the pH_{PZC} estimations were performed in both acidic and basic aqueous phases at different pH values. A series of 30 mL of (0.1 M) KNO_3 aqueous solution were taken into 100 mL conical flasks, and their pH values were adjusted to values between 2 and 10 (2, 4, 6, 8, and 10) by adding 0.1 M HCl and 0.1 M NaOH. Afterward, 15 mg of adsorbent **1** was added in each conical flask for 24 h. Now, after the completion of this time period, the

Scheme 2. Schematic Representation of Encapsulation of NPs inside the Pores of the MOF
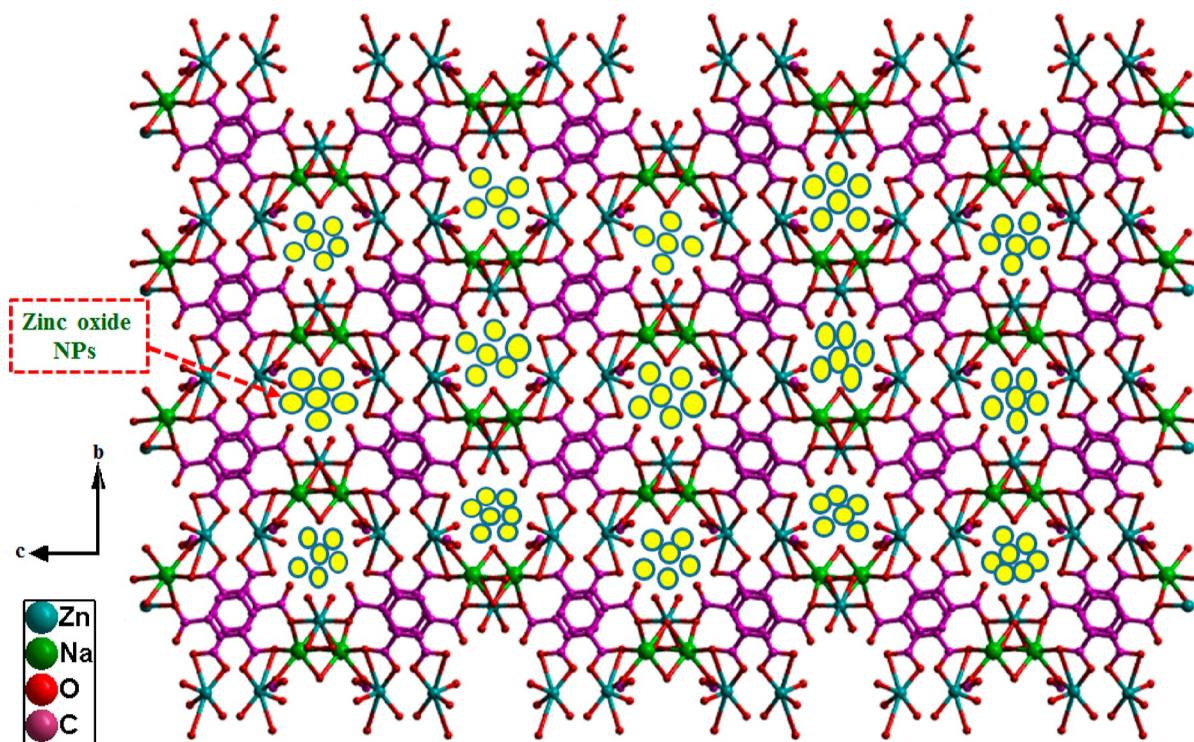
solutions were centrifuged, and their pH (final pH) values were measured.[91,92]

ASSOCIATED CONTENT

Supporting Information

The Supporting Information is available free of charge at https://pubs.acs.org/doi/10.1021/acsomega.2c01869.

> New topology of the 3,4,5,5-c net in the standard representation of structure **1**, IR spectra of **1**, ZnO NPs, and ZnO@**1**, PXRD patterns of **1**, simulated and as-synthesized ZnO@**1** after photocatalysis and after dye adsorption, thermogravimetric curves of **1** and ZnO@**1**, BET isotherm and pore volume of **1**, UV−vis spectra of MO with the indication of a negligible amount of adsorption, a plausible mechanism for dye adsorption over **1**, multilevel analysis of molecular complex packing as a monomer of **1**, properties of dye molecules with the reference, crystal data and structural refinement for **1**, and bond lengths and bond angles of **1** (PDF)

> Single-crystal data of **1** (DOI:) with CCDC 2119993This data can be obtained free of charge via http://www.ccdc.cam.ac.uk/conts/retrieving.html, or from the Cambridge Crystallographic Data Centre, 12 Union Road, Cambridge CB2 1EZ, UK; Fax: (+44) 1223-336-033; or Email:deposit@ccdc.cam.ac.uk (CIF)

AUTHOR INFORMATION

Corresponding Author

Musheer Ahmad − *Department of Applied Chemistry, ZHCET, Faculty of Engineering and Technology, Aligarh Muslim University, Aligarh, Uttar Pradesh 202002, India;* orcid.org/0000-0002-7446-0232; Phone: +91 9760511991; Email: amusheer4@gmail.com

Authors

Arif Ali − *Department of Applied Chemistry, ZHCET, Faculty of Engineering and Technology, Aligarh Muslim University, Aligarh, Uttar Pradesh 202002, India*

Mohd Muslim − *Department of Applied Chemistry, ZHCET, Faculty of Engineering and Technology, Aligarh Muslim University, Aligarh, Uttar Pradesh 202002, India*

Ishita Neogi − *Chemical Sciences and Technology Division, CSIR-National Institute for Interdisciplinary Science and Technology (NIIST), Thiruvananthapuram 695019, India;* orcid.org/0000-0002-1668-3657

Mohd Afzal − *Department of Chemistry, College of Science, King Saud University, Riyadh 11451, Saudi Arabia*

Abdullah Alarifi − *Department of Chemistry, College of Science, King Saud University, Riyadh 11451, Saudi Arabia*

Complete contact information is available at:
https://pubs.acs.org/10.1021/acsomega.2c01869

Notes

The authors declare no competing financial interest.

REFERENCES

(1) Munir, M.; Nazar, M. F.; Zafar, M. N.; Zubair, M.; Ashfaq, M.; Hosseini-Bandegharaei, A.; Khan, S. U.-D.; Ahmad, A. Effective

Adsorptive Removal of Methylene Blue from Water by Didodecyldimethylammonium Bromide-Modified Brown Clay. *ACS Omega* **2020**, *5*, 16711−16721.

(2) Rehman, M. S. U.; Munir, M.; Ashfaq, M.; Rashid, N.; Nazar, M. F.; Danish, M.; Han, J.-I. Adsorption of Brilliant Green dye from aqueous solution onto red clay. *Chem. Eng. J.* **2013**, *228*, 54−62.

(3) Dong, J.-P.; Shi, Z.-Z.; Li, B.; Wang, L.-Y. Synthesis of a novel 2D zinc(II) metal−organic framework for photocatalytic degradation of organic dyes in water. *Dalton Trans.* **2019**, *48*, 17626.

(4) Kant, R. Textile dyeing industry an environmental hazard. *J. Nat. Sci. Res.* **2012**, *04*, 22−26.

(5) Ajmal, A.; Majeed, I.; Malik, R. N.; Idriss, H.; Nadeem, M. A. Principles and mechanisms of photocatalytic dye degradation on TiO2 based photocatalysts: a comparative overview. *RSC Adv.* **2014**, *4*, 37003−37026.

(6) Bensalah, N.; Alfaro, M. A. Q.; Martínez-Huitle, C. A. Electrochemical treatment of synthetic wastewaters containing Alphazurine A dye. *Chem. Eng. J.* **2009**, *149*, 348−352.

(7) Auta, M.; Hameed, B. H. Preparation of waste tea activated carbon using potassium acetate as an activating agent for adsorption of Acid Blue 25 dye. *Chem. Eng. J.* **2011**, *171*, 502−509.

(8) Muslim, M.; Ali, A.; Neogi, I.; Dege, N.; Shahid, M.; Ahmad, M. Facile synthesis, topological study, and adsorption properties of a novel Co(II)-based coordination polymer for adsorptive removal of methylene blue and methyl orange dyes. *Polyhedron* **2021**, *210*, 115519.

(9) Zhang, M.; Wang, L.; Zeng, T.; Shang, Q.; Zhou, H.; Pan, Z.; Cheng, Q. Two pure MOF-photocatalysts readily prepared for the degradation of methylene blue dye under visible light. *Dalton Trans.* **2018**, *47*, 4251−4258.

(10) Fan, W.; Gao, W.; Zhang, C.; Tjiu, W. W.; Pan, J.; Liu, T. Hybridization of graphene sheets and carbon-coated Fe3O4 nanoparticles as a synergistic adsorbent of organic dyes. *J. Mater. Chem.* **2012**, *22*, 25108−25115.

(11) Yaseen, D. A.; Scholz, M. Textile dye wastewater characteristics and constituents of synthetic effluents: a critical review. *Int. J. Environ. Sci. Technol.* **2019**, *16*, 1193−1226.

(12) Howarth, A. J.; Liu, Y.; Li, P.; Li, Z.; Wang, T. C.; Hupp, J. T.; Farha, O. K. Chemical, thermal and mechanical stabilities of metal−organic frameworks. *Nat. Rev. Mater.* **2016**, *1*, 15018.

(13) Lin, Z.-J.; Lü, J.; Hong, M.; Cao, R. Metal−organic frameworks based on flexible ligands (FL-MOFs): Structures and applications. *Chem. Soc. Rev.* **2014**, *43*, 5867−5895.

(14) Pang, Q.; Tu, B.; Li, Q. Metal−organic frameworks with multicomponents in order. *Coord. Chem. Rev.* **2019**, *388*, 107−125.

(15) Zhou, H.-C.; Long, J. R.; Yaghi, O. M. Introduction to metal−organic frameworks. *Chem. Rev.* **2012**, *112*, 673−674.

(16) Sun, T.; Xu, L.; Wang, D.; Li, Y. Metal organic frameworks derived single atom catalysts for electrocatalytic energy conversion. *Nano Res.* **2019**, *12*, 2067−2080.

(17) Reddy, C. V.; Reddy, K. R.; Harish, V. V. N.; Shim, J.; Shankar, M. V.; Shetti, N. P.; Aminabhavi, T. M. Metal-organic frameworks (MOFs)-based efficient heterogeneous photocatalysts: Synthesis, properties and its applications in photocatalytic hydrogen generation, CO₂ reduction and photodegradation of organic dyes. *Int. J. Hydrogen Energy* **2020**, *45*, 7656−7679.

(18) Rojas, S.; Horcajada, P. Metal-Organic Frameworks for the Removal of Emerging Organic Contaminants in Water. *Chem. Rev.* **2020**, *120*, 8378−8415.

(19) Ma, X.; Liu, H.; Yang, W.; Mao, G.; Zheng, L.; Jiang, H.-L. Modulating Coordination Environment of Single-Atom Catalysts and Their Proximity to Photosensitive Units for Boosting MOF Photocatalysis. *J. Am. Chem. Soc.* **2021**, *143*, 12220−12229.

(20) (a) Singh, A.; Singh, A. K.; Liu, J.; Kumar, A. Syntheses, design strategies, and photocatalytic charge dynamics of metal−organic frameworks (MOFs): a catalyzed photo-degradation approach towards organic dyes. *Catal. Sci. Technol.* **2021**, *11*, 3946−3989. (b) Zeng, L.; Guo, X.; He, C.; Duan, C. Metal−Organic Frameworks: Versatile Materials for Heterogeneous Photocatalysis. *ACS Catal.* **2016**, *6*, 7935−7947.

(21) Samanta, D.; Verma, P.; Roy, S.; Maji, T. K. Nanovesicular MOF with Omniphilic Porosity: Bimodal Functionality for White-Light Emission and Photocatalysis by Dye Encapsulation. *ACS Appl. Mater. Interfaces* **2018**, *10*, 23140−23146.

(22) (a) Esrafili, L.; Firuzabadi, F. D.; Morsali, A.; Hu, M.-L. Reuse of Predesigned Dual-Functional Metal Organic Frameworks (DF-MOFs) after Heavy Metal Removal. *J. Hazard. Mater.* **2021**, *403*, 123696. (b) Shahnawaz Khan, M.; Khalid, M.; Shahid, M. What triggers dye adsorption by metal organic frameworks? The current perspectives. *Mater. Adv.* **2020**, *1*, 1575−1601.

(23) (a) Zhong, Y.; Chen, C.; Liu, S.; Lu, C.; Liu, D.; Pan, Y.; Sakiyama, H.; Muddassir, M.; Liu, J. A new magnetic adsorbent of eggshell-zeolitic imidazolate framework for highly efficient removal of norfloxacin. *Dalton Trans.* **2021**, *50*, 18016−18026. (b) Chi, H.-Y.; Hung, S.-H.; Kan, M.-Y.; Lee, L.-W.; Lam, C. H.; Chen, J.-J.; Kang, D.-Y. Metal−organic frameworks for dye sorption: structure−property relationships and scalable deposition of the membrane adsorber. *CrystEngComm* **2018**, *20*, 5465−5474.

(24) (a) Wang, J.; Zhou, L.; Rao, C.; Wang, G.-L.; Jiang, F.; Singh, A.; Kumar, A.; Liu, J. Two 3D supramolecular isomeric Zn(II)-MOFs as photocatalysts for photodegradation of methyl violet dye. *Dyes Pigm.* **2021**, *190*, 109285. (b) Liu, Y.; Wang, S.; Lu, Y.; Zhao, Y.; Zhang, Y.; Xu, G.; Zhang, J.; Fang, Z.; Xu, W.; Chen, X. Loading Control of Metal−Organic Frameworks in Fe3O4@MOFs Series Composite Adsorbents for Optimizing Dye Adsorption. *Ind. Eng. Chem. Res.* **2019**, *58*, 22244−22249.

(25) (a) Fu, H.-R.; Wang, N.; Qin, J.-H.; Han, M.-L.; Ma, L.-F.; Wang, F. Spatial confinement of a cationic MOF: a SC−SC approach for high capacity Cr(vi)-oxyanion capture in aqueous solution. *Chem. Commun.* **2018**, *54*, 11645−11648. (b) Lee, H. J.; Choi, S.; Oh, M. Well-dispersed hollow porous carbon spheres synthesized by direct pyrolysis of core−shell type metal− organic frameworks and their sorption properties. *Chem. Commun.* **2014**, *50*, 4492−4495. (c) Zhao, Y.; Wang, L.; Fan, N.-N.; Han, M.-L.; Yang, G.-P.; Ma, L.-F. Porous Zn(II)-Based Metal−Organic Frameworks Decorated with Carboxylate Groups Exhibiting High Gas Adsorption and Separation of Organic Dyes. *Cryst. Growth Des.* **2018**, *18*, 7114−7121.

(26) Ahmed, A.; Ali, A.; Ahmed, M.; Parida, K. N.; Ahmad, M.; Ahmad, A. Construction and topological studies of a three-dimensional (3D) coordination polymer showing selective adsorption of aromatic hazardous dyes. *Sep. Purif. Technol.* **2021**, *265*, 118482.

(27) Aijaz, A.; Fujiwara, N.; Xu, Q. From Metal-Organic Framework to Nitrogen-Decorated Nanoporous Carbons: High CO₂ Uptake and Efficient Catalytic Oxygen Reduction. *J. Am. Chem. Soc.* **2014**, *136*, 6790−6793.

(28) Sen, S.; Neogi, S.; Aijaz, A.; Xu, Q.; Bharadwaj, P. K. Construction of Non- Interpenetrated Charged Metal-Organic Frameworks with Doubly-Pillared Layers: Pore Modification and Selective Gas Adsorption. *Inorg. Chem.* **2014**, *53*, 7591−7598.

(29) He, H.; Zhang, D.-Y.; Guo, F.; Sun, F. A Versatile Microporous Zinc(II) Metal−Organic Framework for Selective Gas Adsorption, Cooperative Catalysis, and Luminescent Sensing. *Inorg. Chem.* **2018**, *57*, 7314−7320.

(30) Liang, Y.-J.; Yao, J.; Deng, M.; Liu, Y.-E.; Xu, Q.-Q.; Li, Q.-X.; Jing, B.; Zhu, A.-X.; Huang, B. A porous anionic zinc(II) metal−organic framework for gas adsorption, selective uptake of dyes and sensing of Fe³⁺ by Tb³⁺ ion encapsulation. *CrystEngComm* **2021**, *23*, 7348−7357.

(31) (a) Hu, M.-L.; Joharian, M.; Razavi, S. A. A.; Morsali, A.; Wu, D.-Z.; Azhdari Tehrani, A.; Wang, J.; Junk, P. C.; Guo, Z.-F. Phenolic nitroaromatics detection by fluorinated metal-organic frameworks: Barrier elimination for selective sensing of specific group of nitroaromatics. *J. Hazard. Mater.* **2021**, *406*, 124501. (b) Kumar, P.; Deep, A.; Kim, K.-H. Metal organic frameworks for sensing applications. *TrAC Trends in Analytical Chemistry* **2015**, *73*, 39−53.

(32) Kreno, L. E.; Leong, K.; Farha, O. K.; Allendorf, M.; Van Duyne, R. P.; Hupp, J. T. Metal−Organic Framework Materials as Chemical Sensors. *Chem. Rev.* **2012**, *112*, 1105−1125.

(33) Li, H.-Y.; Zhao, S.-N.; Zang, S.-Q.; Li, J. Functional metal—organic frameworks as effective sensors of gases and volatile compounds. *Chem. Soc. Rev.* **2020**, *49*, 6364−6401.

(34) Agarwal, R. A.; Aijaz, A.; Ahmad, M.; Sañudo, E. C.; Xu, Q.; Bharadwaj, P. K. Two New Coordination Polymers with Co(II) and Mn(II): Selective Gas Adsorption and Magnetic Studies. *Cryst. Growth Des.* **2012**, *12*, 2999−3005.

(35) Kamaal, S.; Gupta, M.; Mishra, R.; Ali, A.; Alarifi, A.; Afzal, M.; Das, R.; Ahmad, M. A Three-Dimensional Pentanuclear Co(II) Coordination Polymer: Structural Topology, Hirshfeld Surface Analysis and Magnetic Properties. *ChemistrySelect* **2020**, *5*, 13732−13737.

(36) Thorarinsdottir, A. E.; Harris, T. D.; Harris, T. D. Metal—Organic Framework Magnets. *Chem. Rev.* **2020**, *120*, 8716−8789.

(37) Falcaro, P.; Lapierre, F.; Marmiroli, B.; Styles, M.; Zhu, Y.; Takahashi, M.; Hill, A. J.; Doherty, C. M. Positioning an individual metal—organic framework particle using a magnetic field. *J. Mater. Chem. C* **2013**, *1*, 42−45.

(38) Kamaal, S.; Alam, M. J.; Afzal, M.; Ali, A.; Ahmad, S.; Alarifi, A.; Das, R.; Gupta, M.; Ahmad, M. Fabrication of a new 2D Co(II)- organic framework tuned by semi-flexible dicarboxylate and 1,4-bis(4-pyridinylmethyl)piperazine ligands: Topology, DFT/UB3LYP calculations, Hirshfeld surface analysis and magnetic studies. *J. Mol. Struct.* **2021**, *1229*, 129616.

(39) Wang, Q.; Astruc, D. State of the Art and Prospects in Metal—Organic Framework (MOF)-Based and MOF-Derived Nanocatalysis. *Chem. Rev.* **2020**, *120*, 1438−1511.

(40) Baumann, A. E.; Burns, D. A.; Liu, B.; Thoi, V. S. Metal-organic framework functionalization and design strategies for advanced electrochemical energy storage devices. *Commun. Chem.* **2019**, *2*, 1−14.

(41) Zhang, S.-R.; Li, J.; Du, D.-Y.; Qin, J.-S.; Li, S.-L.; He, W.-W.; Su, Z.-M.; Lan, Y.-Q.; Lan, Y.-Q. A multifunctional microporous anionic metal—organic framework for column- chromatographic dye separation and selective detection and adsorption of Cr3+. *J. Mater. Chem. A* **2015**, *3*, 23426−23434.

(42) (a) Li, Y.; Gao, C.; Jiao, J.; Cui, J.; Li, Z.; Song, Q. Selective Adsorption of Metal—Organic Framework toward Methylene Blue: Behavior and Mechanism. *ACS Omega* **2021**, *6*, 33961−33968. (b) Abedi, M.; Mahmoudi, G.; Hayati, P.; Machura, B.; Zubkov, F. I.; Mohammadi, K.; Bahrami, S.; Derikvandi, H.; Mehrabadi, Z.; Kirillov, A. M. A 3D heterometallic Ni(ii)/K(i) MOF with a rare rna topology: synthesis, structural features, and photocatalytic dye degradation modeling. *New J. Chem.* **2019**, *43*, 17457−17465.

(43) (a) Ishida, T.; Nagaoka, M.; Akita, T.; Haruta, M. Deposition of Gold Clusters on Porous Coordination Polymers by Solid Grinding and Their Catalytic Activity in Aerobic Oxidation of Alcohols. *Chem.—Eur. J.* **2008**, *14*, 8456−8460. (b) Ishida, T.; Kawakita, N.; Akita, T.; Haruta, M. One-pot N-alkylation of primary amines to secondary amines by gold clusters supported on porous coordination polymers. *Gold Bull.* **2009**, *42*, 267−274. (c) Jiang, H.-L.; Lin, Q.-P.; Akita, T.; Liu, B.; Ohashi, H.; Oji, H.; Honma, T.; Takei, T.; Haruta, M.; Xu, Q. Ultrafine Gold Clusters Incorporated into a Metal-Organic Framework. *Chem.—Eur. J.* **2011**, *17*, 78−81. (d) Mukoyoshi, M.; Kobayashi, H.; Kusada, K.; Hayashi, M.; Yamada, T.; Maesato, M.; Taylor, J. M.; Kubota, Y.; Kato, K.; Takata, M.; Yamamoto, T.; Matsumura, S.; Kitagawa, H. Hybrid materials of Ni NP@MOF prepared by a simple synthetic method. *Chem. Commun.* **2015**, *51*, 12463−12466.

(44) Chen, L.; Zhan, W.; Fang, H.; Cao, Z.; Yuan, C.; Xie, Z.; Kuang, Q.; Zheng, L. Selective Catalytic Performances of Noble Metal Nanoparticle@MOF Composites: The Concomitant Effect of Aperture Size and Structural Flexibility of MOF Matrices. *Chem.—Eur. J.* **2017**, *23*, 11397−11403.

(45) Chen, Y.-Z.; Zhou, Y.-X.; Wang, H.; Lu, J.; Uchida, T.; Xu, Q.; Yu, S.-H.; Jiang, H.-L. Multifunctional PdAg@MIL-101 for One-Pot Cascade Reactions: Combination of Host— Guest Cooperation and Bimetallic Synergy in Catalysis. *ACS Catal.* **2015**, *5*, 2062−2069.

(46) Chen, Y.-Z.; Wang, Z. U.; Wang, H.; Lu, J.; Yu, S.-H.; Jiang, H.-L. Singlet Oxygen- Engaged Selective Photo-Oxidation over PtNanocrys-tals/Porphyrinic MOF: The Roles of Photothermal Effect and Pt Electronic State. *J. Am. Chem. Soc.* **2017**, *139*, 2035−2044.

(47) Yang, Q.; Xu, Q.; Jiang, H.-L. Metal−organic frameworks meet metal nanoparticles: synergistic effect for enhanced catalysis. *Chem. Soc. Rev.* **2017**, *46*, 4774−4808.

(48) Serezhkin, V. N.; Vologzhanina, A. V.; Serezhkina, L. B.; Smirnova, E. S.; Grachova, E. V.; Ostrova, P. V.; Antipin, M. Y. Crystallochemical formula as a tool for describing metal— ligand complexes − a pyridine-2,6-dicarboxylate example. *Acta Crystallogr., Sect. B: Struct. Sci.* **2009**, *65*, 45−53.

(49) Park, J. Y.; Woon, D. E. Theortical modeling of formic acid (HCOOH), fomate(HCOO⁻), and ammonium (NH₄⁺) vibrational spectra in astrophysical ices. *Astrophys. J.* **2006**, *648*, 1285−1290.

(50) Punnoose, A.; Dodge, K.; Rasmussen, J. W.; Chess, J.; Wingett, D.; Anders, C. Cytotoxicity of ZnO Nanoparticles Can Be Tailored by Modifying Their Surface Structure: A Green Chemistry Approach for Safer Nanomaterials. *ACS Sustainable Chem. Eng.* **2014**, *2*, 1666−1673.

(51) Bian, S.-W.; Mudunkotuwa, I. A.; Rupasinghe, T.; Grassian, V. H. Aggregation and dissolution of 4 nm ZnO nanoparticles in aqueous environments: Influence of pH, ionic strength, size, and adsorption of humic acid. *Langmuir* **2011**, *27*, 6059−6068.

(52) Max, J.-J.; Chapados, C. Infrared spectroscopy of aqueous carboxylic acids: Comparison between different acids and their salts. *J. Phys. Chem. A* **2004**, *108*, 3324−3337.

(53) (a) Hermes, S.; Schröder, F.; Amirjalayer, S.; Schmid, R.; Fischer, R. A. Loading of porous metal—organic open frameworks with organometallic CVD precursors: inclusion compounds of the type [LnM]a@MOF-5. *J. Mater. Chem.* **2006**, *16*, 2464−2472. (b) Schröder, F.; Esken, D.; Cokoja, M.; van den Berg, M. W. E.; Lebedev, O. I.; Van Tendeloo, G.; Walaszek, B.; Buntkowsky, G.; Limbach, H.-H.; Chaudret, B.; Fischer, R. A. Ruthenium Nanoparticles inside Porous [Zn4O(bdc)3] by Hydrogenolysis of Adsorbed [Ru(cod)(cot)]: A Solid-State Reference System for Surfactant-Stabilized Ruthenium Colloids. *J. Am. Chem. Soc.* **2008**, *130*, 6119−6130.

(54) Faisal, S.; Jan, H.; Shah, S. A.; Shah, S.; Khan, A.; Akbar, M. T.; Rizwan, M.; Jan, F.; Wajidullah, N.; Akhtar, N.; Khattak, A.; Syed, S. Green Synthesis of Zinc Oxide (ZnO) Nanoparticles Using Aqueous Fruit Extracts of Myristicafragrans: Their Characterizations and Biological and Environmental Applications. *ACS Omega* **2021**, *6*, 9709−9722.

(55) Kupgan, G.; Liyana-Arachchi, T. P.; Colina, C. M. NLDFT Pore Size Distribution in Amorphous Microporous Materials. *Langmuir* **2017**, *33*, 11138−11145.

(56) Zhou, Y.; Zhang, Y.; Xu, X.; Zhao, S.; Guo, Z.; Wu, K.-H.; Tan, C.; Wang, Z. Bimetallic Metal-Organic Framework Derived Metal-Carbon Hybrid for Efficient Reversible Oxygen Electrocatalysis. *Front. Chem.* **2019**, *7*, 747.

(57) (a) Arora, C.; Soni, S.; Sahu, S.; Mittal, J.; Kumar, P.; Bajpai, P. K. Iron Based Metal Organic Framework for Efficient Removal of Methylene Blue Dye from Industrial Waste. *J. Mol. Liq.* **2019**, *284*, 343−352. (b) Han, Y.; Liu, M.; Li, K.; Sun, Q.; Zhang, W.; Song, C.; Zhang, G.; Conrad Zhang, Z.; Guo, X. In situ synthesis of titanium doped hybrid metal—organic framework UiO-66 with enhanced adsorption capacity for organic dyes. *Inorg. Chem. Front.* **2017**, *4*, 1870−1880.

(58) Kim, S.-H.; Choi, P.-P. Enhanced Congo red dye removal from aqueous solutions using iron nanoparticles: adsorption, kinetics, and equilibrium studies. *Dalton Trans.* **2017**, *46*, 15470−15479.

(59) Molavi, H.; Hakimian, A.; Shojaei, A.; Raeiszadeh, M. Selective dye adsorption by highly water stable metal-organic framework: long term stability analysis in aqueous media. *Appl. Surf. Sci.* **2018**, *445*, 424−436.

(60) (a) Maity, K.; Kundu, T.; Banerjee, R.; Biradha, K. One-dimensional water cages with repeat units of IJH2O)24 resembling pagodane trapped in a 3Dcoordination polymer: proton conduction and tunable luminescence emission by adsorption of anionic dyes. *CrystEngComm* **2015**, *17*, 4439−4443. (b) Hosseinzadeh, H.; Abdi, K. Efficient Removal of Methylene Blue Using a Hybrid Organic—Inorganic Hydrogel Nanocomposite Adsorbent Based on Sodium

Alginate− Silicone Dioxide. *J. Inorg. Organomet. Polym. Mater.* **2017**, 27, 1595−1612. (c) Ji, Y.; Ma, C.; Li, J.; Zhao, H.; Chen, Q.; Li, M.; Liu, H. A Magnetic Adsorbent for the Removal of Cationic Dyes from Wastewater. *Nanomaterials* **2018**, 8, 710.

(61) (a) Wu, M. Z.; Shi, J. Y.; Chen, P. Y.; Tian, L.; Chen, J. Two 3D Cobalt(II) Metal- Organic Frameworks with Micropores for Selective Dye Adsorption. *Inorg. Chem.* **2019**, 58, 3130−3136. (b) Saleh, H. A. M.; Mantasha, I.; Qasem, K. M. A.; Shahid, M.; Akhtar, M. N.; AlDamen, M. A.; Ahmad, M. A Two Dimensional Co(II) Metal−Organic Framework with Bey Topology for Excellent Dye Adsorption and Separation: Exploring Kinetics and Mechanism of Adsorption. *Inorganica Chim. Acta* **2020**, 512, 119900. (c) Aljeboree, A. M.; Alshirifi, A. N.; Alkaim, A. F. Kinetics and Equilibrium Study for the Adsorption of Textile Dyes on Coconut Shell Activated Carbon. *Arab. J. Chem.* **2017**, 10, S3381−S3393. (d) Banerjee, S.; Chattopadhyaya, M. C. Adsorption Characteristics for the Removal of a Toxic Dye, Tartrazine from Aqueous Solutions by a Low Cost Agricultural by-Product. *Arab. J. Chem.* **2017**, 10, S1629−S1638.

(62) Xue, Z.-Z.; Guan, Q.-W.; Xu, L.; Meng, X.-D.; Pan, J. A Zn(II)-Based Coordination Polymer Featuring Selective Detection of Fe3+ and Efficient Capture of Anionic Dyes. *Cryst. Growth Des.* **2020**, 20, 7477−7483.

(63) Patel, U.; Parmar, B.; Dadhania, A.; Suresh, E. Zn(II)/Cd(II)-Based Metal−Organic Frameworks as Bifunctional Materials for Dye Scavenging and Catalysis of Fructose/Glucose to 5-Hydroxymethyl-furfural. *Inorg. Chem.* **2021**, 60, 9181−9191.

(64) (a) Al-Harby, N. F.; Albahly, E. F.; Mohamed, N. A. Kinetics, Isotherm and Thermodynamic Studies for Efficient Adsorption of Congo Red Dye from Aqueous Solution onto Novel Cyanoguanidine-Modified Chitosan Adsorbent. *Polymers* **2021**, 13, 4446. (b) Gao, Y.; Li, Y.; Liang, C.; Cen, P.; Xi, J.; Guo, Y.; Song, W.; Liu, X. Two mesoporous anionic metal−organic frameworks for selective and efficient adsorption of a cationic organic dye. *Dalton Trans.* **2021**, 50, 17603−17610. (c) Li, Q.; Qian, J.; Du, L.; Zhao, Q. Zinc-Tetracarboxylate Framework Material with Nano-Cages and One- Dimensional Channels for Excellent Selective and Effective Adsorption of Methyl Blue Dye. *RSC Adv.* **2020**, 10, 3539−3543.

(65) Kamal, S.; Khalid, M.; Shahnawaz Khan, M.; Ashafaq, M.; I, M.; Shahwaz Ahmad, M.; Ahmad, M.; Faizan, M.; Ahmad, S. Synthesis, Characterization and DFT Studies of Water Stable Cd(II) Metal−Organic Clusters with Better Adsorption Property towards the Organic Pollutant in Waste Water. *Inorganica Chim. Acta* **2020**, 512, 119872.

(66) Haque, E.; Jun, J. W.; Jhung, S. H. Adsorptive removal of methyl orange and methylene blue from aqueous solution with a metal-organic framework material, iron terephthalate (MOF-235). *J. Hazard. Mater.* **2011**, 185, 507−511.

(67) Mahto, T. K.; Chandra, S.; Haldar, C.; Sahu, S. K. Kinetic and thermodynamic study of polyaniline functionalized magnetic meso-porous silica for magnetic field guided dye adsorption. *RSC Adv.* **2015**, 5, 47909−47919.

(68) Uddin, M. J.; Ampiaw, R. E.; Lee, W. Adsorptive removal of dyes from wastewater using a metal-organic framework: A review. *Chemosphere* **2021**, 284, 131314.

(69) (a) Jun, B.-M.; Heo, J.; Taheri-Qazvini, N.; Park, C. M.; Yoon, Y. Adsorption of selected dyes on Ti3C2Tx MXene and Al-based metal-organic framework. *Ceram. Int.* **2020**, 46, 2960−2968. (b) Mondal, S.; Dastidar, P. Zn(II)- Coordination Polymers with a Right- And Left-Handed Twist: Multifunctional Metal- Organic Hybrid for Dye Adsorption and Drug Delivery. *Cryst. Growth Des.* **2020**, 20, 7411−7420. (c) Ahamad, M. N.; Khan, M. S.; Shahid, M.; Ahmad, M. Metal Organic Frameworks Decorated with Free Carboxylic Acid Groups: Topology, Metal Capture and Dye Adsorption Properties. *Dalt. Trans.* **2020**, 49, 14690−14705.

(70) Saeed, T.; Naeem, A.; Din, I. U.; Farooq, M.; Khan, I. W.; Hamayun, M.; Malik, T. Synthesis of chitosan composite of metal-organic framework for the adsorption of dyes; kinetic and thermodynamic approach. *J. Hazard Mater.* **2022**, 427, 127902.

(71) (a) Salleh, M. A. M.; Mahmoud, D. K.; Karim, W. A. W. A.; Idris, A. Cationic and anionic dye adsorption by agricultural solid wastes: a

comprehensive review. *Desalination* **2011**, 280, 1−13. (b) Choi, J.-W.; Park, Y.-J.; Choi, S.-J. Synthesis of Metal−Organic Framework ZnOx-MOF@MnO2 Composites for Selective Removal of Strontium Ions from Aqueous Solutions. *ACS Omega* **2020**, 5, 8721−8729. (c) Paiman, S. H.; Rahman, M. A.; Uchikoshi, T.; Abdullah, N.; Othman, M. H. D.; Jaafar, J.; Abas, K. H.; Ismail, A. F. Functionalization Effect of Fe-Type MOF for Methylene Blue Adsorption. *J. Saudi Chem. Soc.* **2020**, 24, 896−905. (d) Haque, E.; Jun, J. W.; Jhung, S. H. Adsorptive Removal of Methyl Orange and Methylene Blue from Aqueous Solution with a Metal-Organic Framework Material, Iron Terephthalate (MOF- 235). *J. Hazard. Mater.* **2011**, 185, 507−511.

(72) (a) Russo, V.; Hmoudah, M.; Broccoli, F.; Iesce, M. R.; Jung, O.-S.; Di Serio, M. Applications of Metal Organic Frameworks in Wastewater Treatment: A Review on Adsorption and Photo-degradation. *Front. Chem. Eng.* **2020**, 2, 581487. (b) Abdi, J.; Vossoughi, M.; Mahmoodi, N. M.; Alemzadeh, I. Synthesis of metal-organic framework hybrid nanocomposites based on GO and CNT with high adsorption capacity for dye removal. *Chem. Eng. J.* **2017**, 326, 1145−1158.

(73) Zhang, J.; Li, F.; Sun, Q. Rapid and selective adsorption of cationic dyes by a unique metal- organic framework with decorated pore surface. *Appl. Surf. Sci.* **2018**, 440, 1219−1226.

(74) (a) Liu, W.-b.; Cui, G.-N.; Wang, H.; Zhang, D.-M.; Wu, R.-X.; Li, L.; Zhang, X.; Fan, Y.-H. Efficient and selective adsorption of dye in aqueous environment employing a functional Zn(II)-based metal organic framework. *J. Solid State Chem.* **2020**, 292, 121740. (b) Ahmad, R.; Ansari, K. Novel in-situ fabrication of L-methionine functionalized bionanocomposite for adsorption of Amido Black 10B dye. *Process Biochem.* **2022**, 119, 48−57.

(75) Zhao, X.; Liu, S.; Tang, Z.; Niu, H.; Cai, Y.; Meng, W.; Wu, F.; Giesy, J. P. Synthesis of magnetic metal- organic framework (MOF) for efficient removal of organic dyes from water. *Sci. Rep.* **2015**, 5, 11849.

(76) (a) Wei, X.; Wang, Y.; Chen, J.; Liu, Z.; Xu, F.; He, X.; Li, H.; Zhou, Y. Fabrication of Di-Selective Adsorption Platform Based on Deep Eutectic Solvent Stabilized Magnetic Polydopamine: Achieving Di-Selectivity Conversion through Adding CaCl2. *Chem. Eng. J.* **2021**, 421, 127815. (b) Zhang, J.; Li, F.; Sun, Q. Rapid and selective adsorption of cationic dyes by a unique metal-organic framework with decorated pore surface. *Appl. Surf. Sci.* **2018**, 440, 1219−1226. (c) Zhao, X.; Liu, S.; Tang, Z.; Niu, H.; Cai, Y.; Meng, W. Synthesis of magnetic metal-organic framework (MOF) for efficient removal of organic dyes from water. *Sci Rep* **2015**, 5, 11849.

(77) Alqadami, A. A.; Naushad, M.; Alothman, Z. A.; Ahamad, T. Adsorptive performance of MOF nanocomposite for methylene blue and malachite green dyes: Kinetics, isotherm and mechanism. *J. Environ. Manage.* **2018**, 223, 29−36.

(78) Li, C.; Xiong, Z.; Zhang, J.; Wu, C. The strengthening role of the amino group in metal- organic framework MIL-53 (Al) for methylene blue and malachite green dye adsorption. *J. Chem. Eng. Data* **2015**, 60, 3414−3422.

(79) Kaur, H.; Kumar, R.; Kumar, A.; Krishnan, V.; Koner, R. R. Trifunctional metal−organic platform for environmental remediation: structural features with peripheral hydroxyl groups facilitate adsorption, degradation and reduction processes. *Dalton Trans.* **2019**, 48, 915−927.

(80) Li, Z.-Q.; Zhang, M.; Liu, B.; Guo, C.-Y.; Zhou, M. Rapid fabrication of metal−organic framework thin films using in situ microwave irradiation and its photocatalytic property. *Inorg. Chem. Commun.* **2013**, 36, 241−244.

(81) Rahman, Q. I.; Hasan, S.; Ali, A.; Mehta, S. K.; Raja, N.; Khan, A. R.; Muddassir, M. Synthesis and Characterizations of Nitrogen (N) Doped Strontium Titanate (SrTiO$_3$) Nanoparticles for Enhanced Visible Light Driven Photocatalytic Degradation. *J. Nanosci. Nano-technol.* **2020**, 20, 6475−6481.

(82) Muslim, M.; Ali, A.; Kamaal, S.; Ahmad, M.; Jane Alam, M.; Rahman, Q. I.; Shahid, M. Efficient adsorption and facile photocatalytic degradation of organic dyes over H-bonded proton-transfer complex: An experimental and theoretical approach. *J. Mol. Liq.* **2022**, 347, 117951.

(83) Zhang, L.; Nie, Y.; Hu, C.; Hu, X. Decolorization of methylene blue in layered manganese oxide suspension with H_2O_2. *J. Hazard. Mater.* **2011**, *190*, 780−785.

(84) Zhao, Y.; Li, L.; Liu, Z.-Y.; Ding, B.; Wang, X.-G.; Luo, Y.; Zhao, X.-J.; Yang, E.-C. Water- Stable Zn(II) Coordination Polymers Regulated by Polysubstituted Benzenes and Their Photocatalytic Performance toward Methylene Blue Degradation Dominated by Ligand-Field Effects. *Cryst. Growth Des.* **2021**, *21*, 1218−1232.

(85) Zhu, B.; Song, D.; Jia, T.; Sun, W.; Wang, D.; Wang, L.; Guo, J.; Jin, L.; Zhang, L.; Tao, H. Effective Visible Light-Driven Photocatalytic Degradation of Ciprofloxacin over Flower-like Fe3O4/Bi2WO6 Composites. *ACS Omega* **2021**, *6*, 1647−1656.

(86) Zhang, Y.; Shang, J.; Song, Y.; Rong, C.; Wang, Y.; Huang, W.; Yu, K. Selective Fenton- like oxidation of methylene blue on modified Fe-zeolites prepared via molecular imprinting technique. *Water Sci. Technol.* **2017**, *75*, 659−669.

(87) Pattappan, D.; Vargheese, S.; Kavya, K. V.; Kumar, R. T. R.; Haldorai, Y. Metal-organic frameworks with different oxidation states of metal nodes and aminoterephthalic acid ligand for degradation of Rhodamine B under solar light. *Chemosphere* **2022**, *286*, 131726.

(88) Park, J. G.; Aubrey, M. L.; Oktawiec, J.; Chakarawet, K.; Darago, L. E.; Grandjean, F.; Long, G. J.; Long, J. R. Charge Delocalization and Bulk Electronic Conductivity in the Mixed-Valence Metal−Organic Framework Fe(1,2,3-triazolate)2(BF4)x. *J. Am. Chem. Soc.* **2018**, *140*, 8526−8534.

(89) Day, R. W.; Bediako, D. K.; Rezaee, M.; Parent, L. R.; Skorupskii, G.; Arguilla, M. Q.; Hendon, C. H.; Stassen, I.; Gianneschi, N. C.; Kim, P.; Dincă, M. Single Crystals of Electrically Conductive Two-Dimensional Metal−Organic Frameworks: Structural and Electrical Transport Properties. *ACS Cent. Sci.* **2019**, *5*, 1959−1964.

(90) Calvo, J. J.; Angel, S. M.; So, M. C. Charge transport in metal−organic frameworks for electronics applications. *APL Mater.* **2020**, *8*, 050901.

(91) Ghosh, M. K.; Pathak, S.; Ghorai, T. K. Synthesis of Two Mononuclear Schiff Base Metal (M = Fe, Cu) Complexes: MOF Structure, Dye Degradation, H2O2 Sensing, and DNA Binding Property. *ACS Omega* **2019**, *4*, 16068−16079.

(92) Sarkar, A.; Adhikary, A.; Mandal, A.; Chakraborty, T.; Das, D. Zn-BTC MOF as an Adsorbent for Iodine Uptake and Organic Dye Degradation. *Cryst. Growth Des.* **2020**, *20*, 7833−7839.

(93) Deng, S.-Q.; Miao, Y.-L.; Tan, Y.-L.; Fang, H.-N.; Li, Y.-T.; Mo, X.-J.; Cai, S.-L.; Fan, J.; Zhang, W.-G.; Zheng, S.-R. An Anionic Nanotubular Metal−Organic Framework for High-Capacity Dye Adsorption and Dye Degradation in Darkness. *Inorg. Chem.* **2019**, *58*, 13979−13987.

(94) K, S. T.; Pavithran, R.; A, V. Design of 3D-supramolecular metal organic framework of zinc as photocatalyst for the degradation of methylene blue through advanced oxidation process. *J. Mol. Struct.* **2021**, *1245*, 131039.

(95) *International Tables for X-ray Crystallography*; Kynoch Press, 1952; Vol. *III*, 257−269.

(96) Dolomanov, O. V.; Bourhis, L. J.; Gildea, R. J.; Howard, J. A. K.; Puschmann, H. OLEX2: a complete structure solution, refinement and analysis program. *Appl. Crystallogr.* **2009**, *42*, 339−341.

(97) Bourhis, L. J.; Dolomanov, O. V.; Gildea, R. J.; Howard, J. A. K.; Puschmann, H. The anatomy of a comprehensive constrained, restrained refinement program for the modern computing environment -Olex2dissected. *Acta Crystallogr., Sect. A: Found. Adv.* **2015**, *71*, 59−75.

(98) Rahman, Q. I.; Ahmad, M.; Misra, S. K.; Lohani, M. Effective photocatalytic degradation of rhodamine B dye by ZnO nanoparticles. *Mater. Lett.* **2013**, *91*, 170−174.